Improvement of the hydrostatic reconstruction scheme to get fully discrete entropy inequalities

Christophe Berthon, Arnaud Duran, Françoise Foucher, Khaled Saleh, Jean de Dieu Zabsonré

Improvement of the hydrostatic reconstruction scheme to get fully discrete entropy inequalities

Christophe Berthon[1], Arnaud Duran[2], Françoise Foucher[3], Khaled Saleh[2], and Jean de Dieu Zabsonré[4]

[1]Laboratoire de Mathématiques Jean Leray, Universit de Nantes, France
[2]Institut Camille Jordan, Université Claude Bernard Lyon 1, France
[3]Laboratoire de Mathématiques Jean Leray, Ecole Centrale de Nantes, France
[4]LAMI, Institut Universitaire de Technologie, Université Nazi BONI, Burkina Faso

Abstract

This work is devoted to the derivation of an energy estimate to be satisfied by numerical schemes when approximating the weak solutions of the shallow water model. More precisely, here we adopt the well-known hydrostatic reconstruction technique to enforce the adopted scheme to be well-balanced; namely to exactly preserve the lake at rest stationary solution. Such a numerical approach is known to get a semi-discrete (continuous in time) entropy inequality. However, a semi-discrete energy estimation turns, in general, to be insufficient to claim the required stability. In the present work, we adopt the artificial numerical viscosity technique to increase the desired stability and then to recover a fully discrete energy estimate. Several numerical experiments illustrate the relevance of the designed viscous hydrostatic reconstruction scheme.

1 Introduction

The present work concerns the derivation of discrete entropy inequalities when adopting the well-known hydrostatic reconstruction technique introduced by Audusse et al [1]. This numerical scheme was proposed to approximate the weak solutions of the shallow-water system. The model under consideration is governed by the following set of partial differential equations:

$$\begin{cases} \partial_t h + \partial_x hu = 0, \\ \partial_t hu + \partial_x \left(hu^2 + g\dfrac{h^2}{2} \right) = -gh\partial_x z, \end{cases} \tag{1}$$

where $h \geq 0$ stands for the water height and $u \in \mathbb{R}$ denotes the water velocity. Here, g is the gravitational constant while z is a given smooth function to represent the bottom topography. For the sake of simplicity in the forthcoming notations, we set

$$w = \begin{pmatrix} h \\ hu \end{pmatrix}, \quad f(w) = \begin{pmatrix} hu \\ hu^2 + g\dfrac{h^2}{2} \end{pmatrix}, \quad \text{and} \quad S(w,z) = \begin{pmatrix} 0 \\ -gh\partial_x z \end{pmatrix}.$$

In addition, we introduce $\Omega \subset \mathbb{R}^2$ the set of physical admissible states given by

$$\Omega = \{w \in \mathbb{R}^2;\ h \geq 0,\ u \in \mathbb{R}\}.$$

From now on, we underline that this admissible state space contains dry areas characterized by $h = 0$. It is well-known that the system (1) is not correctly defined for dry

solutions. However, some numerical simulations may contain dry zones which have to be correctly approximated. In order to deal with wet solutions, far away from dry areas, we also introduce

$$\Omega_0 = \{w \in \mathbb{R}^2;\ h \geq h_0,\ u \in \mathbb{R}\},$$

with $h_0 > 0$ a given constant.

The first-order extracted system from (1) is well-known to be hyperbolic. As a consequence, the Cauchy problem associated with (1) may develop discontinuous solutions in finite time. The discontinuities, the so-called shock waves, are governed by the Rankine-Hugoniot conditions (see [13, 18, 19, 30]) which do not ensure uniqueness of the solution. In order to rule out unphysical solutions, the system is endowed with entropy inequalities (see [13, 29, 41]). Considering the shallow-water model, the entropy inequalities read (see [7]):

$$\partial_t \eta(w) + \partial_x G(w) \leq -ghu\partial_x z, \tag{2}$$

where we have set

$$\eta(w) = h\frac{u^2}{2} + g\frac{h^2}{2} \quad \text{and} \quad G(w) = \left(\frac{u^2}{2} + gh\right) hu. \tag{3}$$

It is worth noticing that $\eta : \Omega_0 \to \mathbb{R}$ is a convex function.

In fact, since z does not depend on time, the above inequality equivalently (see [7]) recasts in an energy estimate as follows:

$$\partial_t \tilde{\eta}(w, z) + \partial_x \tilde{G}(w, z) \leq 0, \tag{4}$$

with

$$\tilde{\eta}(w, z) = \eta(w) + ghz \quad \text{and} \quad \tilde{G}(w, z) = G(w) + ghuz. \tag{5}$$

In addition, the system (1) admits solutions of particular interest; namely the steady state solutions. Since such solutions do not depend on time, they are easily shown to be defined by

$$hu = Q \quad \text{and} \quad \mathcal{B}(w, z) = B, \tag{6}$$

where $\mathcal{B} : \Omega \to \mathbb{R}$ stands for a Bernouilli-like relation given by

$$\mathcal{B}(w, z) = \frac{u^2}{2} + g(h + z). \tag{7}$$

In (6), Q and B are two real constants. Among all the possible steady state solutions, the lake at rest, defined by

$$u = 0 \quad \text{and} \quad h + z = H, \tag{8}$$

with H a given constant, turns out to be of prime importance when deriving numerical schemes to approximate the weak solutions of (1). Indeed, after the work by Bermudez and Vasquez [4] , Greenberg and LeRoux [24] (see also [10, 21, 25, 28]) or Goutal and Maurel [22, 23], it is well-known that a numerical scheme may produce very large errors if it cannot accurately approximate the lake at rest. According to these pioneer works, a scheme able to exactly capture the lake at rest is called a well-balanced scheme.

During the three last decades, numerous strategies have been introduced to correct the failure coming from the non-well-balanced schemes as presented in Figure 1. Among all these (well-balanced) numerical techniques, one is of strong interest, the so called hydrostatic reconstruction procedure introduced in [1]. Indeed, this numerical method can be understood as a very easy way to obtain a well-balanced scheme as soon as a conservative scheme is known to approximate the homogeneous first-order system, for flat topography with z a constant, extracted from (1). To fix the ideas, let us briefly recall the main ingredients in the derivation of the hydrostatic reconstruction.

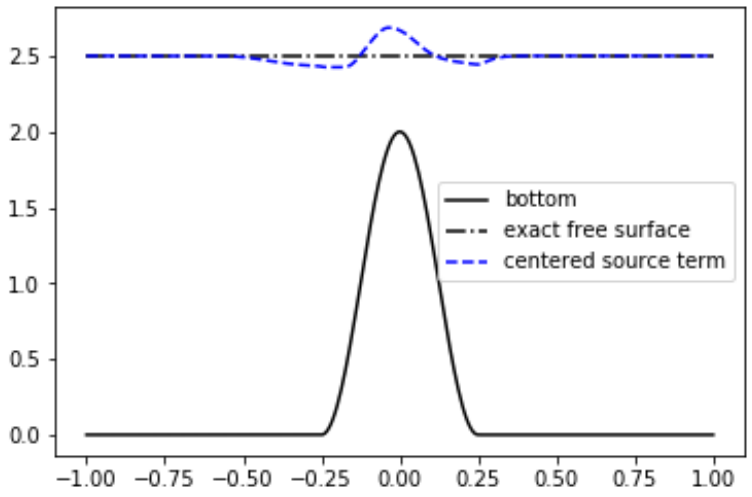

Figure 1: Failure in the lake at rest in the case of an approximation obtained by a HLL Godunov-type scheme to discretize the hyperbolic first-order terms and a centered scheme to discretize the topography source term.

First, we consider a suitable discretization of space and time. To make simple the presentation, the space discretization is assumed to be uniformly made of cells $(x_{i-\frac{1}{2}}, x_{i+\frac{1}{2}})$ with constant size Δx, so that $x_{i+\frac{1}{2}} = x_{i-\frac{1}{2}} + \Delta x$ for all i in $\mathbb{Z}$. Concerning the time discretization, we set $t^{n+1} = t^n + \Delta t$, where $\Delta t > 0$ stands for the time increment which has to be restricted according to a CFL-like condition [18, 32, 45]. Next, we assume known a numerical flux function $\mathcal{F}(w_L, w_R)$ to approximate the flux function $f(w)$ at each interface $x_{i+\frac{1}{2}}$, which is assumed to be consistent as follows:

$$\mathcal{F}(w, w) = f(w) \qquad \forall w \in \Omega.$$

We here do not detail the technique to reach such a numerical flux function and the reader is referred to [20, 27, 39, 40] to get functions $\mathcal{F}$ of Godunov-type, Roe-type, relaxation-type, kinetic-type, etc. In fact, let us emphasize that one of the main asset in the hydrostatic reconstruction approach stays in the opportunity to select any numerical flux function. On each cell $(x_{i-\frac{1}{2}}, x_{i+\frac{1}{2}})$, we introduce water height reconstructions as follows:

$$h^+_{i-\frac{1}{2}} = h^n_i + z_i - z^+_{i-\frac{1}{2}} \quad \text{and} \quad h^-_{i+\frac{1}{2}} = h^n_i + z_i - z^-_{i+\frac{1}{2}}, \tag{9}$$

where $z_i - z^+_{i-\frac{1}{2}} = \mathcal{O}(\Delta x)$ and $z_i - z^-_{i+\frac{1}{2}} = \mathcal{O}(\Delta x)$ are small perturbations. Here, $z^\pm_{i+\frac{1}{2}}$ approximates the topography function on each side of the interface $x_{i+\frac{1}{2}}$. Precise definition of these quantities will be given later on.

Equipped with water height reconstructions, we define the following reconstructed states:

$$w^+_{i-\frac{1}{2}} = \begin{pmatrix} h^+_{i-\frac{1}{2}} \\ h^+_{i-\frac{1}{2}} u^n_i \end{pmatrix} \quad \text{and} \quad w^-_{i+\frac{1}{2}} = \begin{pmatrix} h^-_{i+\frac{1}{2}} \\ h^-_{i+\frac{1}{2}} u^n_i \end{pmatrix} \quad \forall i \in \mathbb{Z}. \tag{10}$$

Then, the hydrostatic reconstruction scheme reads

$$w^{n+1}_i = w^n_i - \frac{\Delta t}{\Delta x}\left(\mathcal{F}(w^-_{i+\frac{1}{2}}, w^+_{i+\frac{1}{2}}) - \mathcal{F}(w^-_{i-\frac{1}{2}}, w^+_{i-\frac{1}{2}})\right) - g\Delta t \begin{pmatrix} 0 \\ \overline{h\partial_x z_i}^n \end{pmatrix}, \tag{11}$$

where the source term discretization is in the following form:

$$\overline{h\partial_x z_i}^n = \overline{h\partial_x z}^+_{i-\frac{1}{2}} + \overline{h\partial_x z}^-_{i+\frac{1}{2}}, \tag{12}$$

for a suitable definition of $\overline{h\partial_x z}^{\pm}_{i+\frac{1}{2}}$ given by

$$\begin{aligned}
\overline{h\partial_x z}^{+}_{i-\frac{1}{2}} &= \frac{1}{2\Delta x}\left(h_i^n + h^+_{i-\frac{1}{2}}\right)\left(z_i - z^+_{i-\frac{1}{2}}\right),\\
\overline{h\partial_x z}^{-}_{i+\frac{1}{2}} &= \frac{1}{2\Delta x}\left(h_i^n + h^-_{i+\frac{1}{2}}\right)\left(z^-_{i+\frac{1}{2}} - z_i\right).
\end{aligned} \tag{13}$$

In fact, the main idea in [1] is enforcing

$$z^-_{i+\frac{1}{2}} = z^+_{i+\frac{1}{2}} \qquad \text{as soon as} \qquad h_i^n + z_i = h_{i+1}^n + z_{i+1}, \tag{14}$$

so that we get

$$h^-_{i+\frac{1}{2}} = h^+_{i+\frac{1}{2}} \qquad \text{as soon as} \qquad h_i^n + z_i = h_{i+1}^n + z_{i+1}. \tag{15}$$

Independently from the choice of the numerical flux function $\mathcal{F}$, the above numerical approach is easily seen to be well-balanced; namely if $u_i^n = 0$ and $h_i^n + z_i = H$ for all $i \in \mathbb{Z}$, then $u_i^{n+1} = 0$ and $h_i^{n+1} + z_i = H$ for all $i \in \mathbb{Z}$.

Now, let us suggest some definitions of the topography $z^{\pm}_{i+\frac{1}{2}}$ at each interface. For instance, in [1], the authors proposed

$$\begin{aligned}
z^-_{i+\frac{1}{2}} &= \min\left(h_i^n + z_i, \max(z_i, z_{i+1})\right),\\
z^+_{i+\frac{1}{2}} &= \min\left(h_{i+1}^n + z_{i+1}, \max(z_i, z_{i+1})\right).
\end{aligned} \tag{16}$$

Next, let us emphasize that several recent works propose extensions of the original hydrostatic reconstruction defined by (16). For instance, in the work by Chen and Noelle [11], the authors suggest to consider

$$z^-_{i+\frac{1}{2}} = \max(z_i, \bar{z}_{i+\frac{1}{2}}) \quad \text{and} \quad z^+_{i+\frac{1}{2}} = \max(z_{i+1}, \bar{z}_{i+\frac{1}{2}})$$

where we have set

$$\bar{z}_{i+\frac{1}{2}} = \min\left(\max(z_i, z_{i+1}), \min(h_i^n + z_i, h_{i+1}^n + z_{i+1})\right).$$

The hydrostatic reconstruction, defined by (9), (10), (11) and (13), turns out to be very easy and fast to be implemented. This makes this procedure very attractive and numerous works apply this technique (for instance, see [3, 6, 14, 15, 33, 34]).

Equipped with well-balanced schemes, an other important property to be satisfied by the scheme concerns the stability. In the present work, we focus on the entropy stability. Indeed, in order to rule out unphysical approximate solutions, it is important that the numerical solution satisfies, in addition, discrete entropy inequalities. We recall that the scheme is said entropy stable if the following strong energy estimation is verified:

$$\begin{aligned}
&\frac{1}{\Delta t}\left(\tilde{\eta}(w_i^{n+1}, z_i) - \tilde{\eta}(w_i^n, z_i)\right)\\
&\qquad + \frac{1}{\Delta x}\left(\tilde{\mathcal{G}}(w^-_{i+\frac{1}{2}}, z_i, w^+_{i+\frac{1}{2}}, z_{i+1}) - \tilde{\mathcal{G}}(w^-_{i-\frac{1}{2}}, z_{i-1}, w^+_{i-\frac{1}{2}}, z_i)\right) \leq 0.
\end{aligned} \tag{17}$$

where $\tilde{\eta}$ is the entropy function defined by (5), and $\tilde{\mathcal{G}}(w_L, z_L, w_R, z_R)$ is the associated numerical entropy flux function consistent with the exact entropy flux, $\tilde{G}$, as follows:

$$\tilde{\mathcal{G}}(w, z, w, z) = \tilde{G}(w, z).$$

In fact, the discrete entropy inequality (17), according to the famous Lax-Wendroff Theorem [31], ensures a convergence to the entropy weak solutions of the system (1) (if the scheme converges).

The derivation of discrete entropy inequality is usually a very difficult task. For instance, in [7–9], relaxation schemes are derived to get entropy stable well-balanced schemes. But, in general, the authors do not address the delicate problem of the full discrete energy estimate (17).

To avoid these difficulties, some works suggest to consider weaker formulations of the entropy stability. For instance, recently in [5,36,37], extensions of the HLL scheme [27] produce entropy consistent schemes (in the sense where entropy inequlity is reached up to $\mathcal{O}(\Delta x)$) able to exactly capture all the steady states (at rest or moving). In [1], the authors establish an entropy inequality satisfied by the semi-discrete (time continuous) scheme associated with the hydrostatic reconstruction (11). Unfortunately, it is well-known that semi-discrete entropy inequalities are not sufficient to obtain a suitable convergence to the entropy weak solution or to get relevant energy estimates. As a consequence, the main question we address here is:

Is it possible to exhibit the entropy inequality (17) for the hydrostatic reconstruction scheme (11)?

In fact, recently in [2], the authors give a negative response. As a consequence, in order to get the expected entropy inequality, the hydrostatic reconstruction scheme (11) must be improved. To address such an issue, the present paper is organized as follows. In the next section, we adopt an artificial viscosity technique as proposed in [12] (see also [42–44]). In fact, by involving additional viscosity, we may expect to increase the stability of the scheme. Moreover, in this work, the required entropy stability is obtained by adopting the well-known entropy criterion introduced by Harten, Lax and van Leer (see Theorem 3.1 page 47 [27]). In order to apply this statement, we also present a Godunov-type reformulation of the derived viscous hydrostatic reconstruction scheme. Section 3 concerns the establishment of the discrete energy estimate (17). To address such an issue, we exhibit the optimal artificial viscosity to minimize the associated entropy dissipation rate. Moreover, we show that the interface topography reconstruction $z^{\pm}_{i+\frac{1}{2}}$ must be given a specific definition. Next, Section 4, we focus on the wet and dry transitions. Clearly, the energy estimate (4) is not well-defined within such a transition. As a consequence, in this section, we introduce an improvement of the derived hydrostatic reconstruction scheme able to deal with wet and dry transition, and preserving the entropy stability requirement far away from vacuum. The last section is devoted to some numerical experiments in order to illustrate the relevance of the herein proposed improvement of the hydrostatic reconstruction method.

2 Viscous hydrostatic reconstruction scheme and Godunov-type reformulation

This section is devoted to an improvement of the hydrostatic reconstruction scheme (11), in order to obtain the required discrete entropy inequality (17). After the pioneer work by Tadmor [42–44] (see also [12,26]), we suggest to introduce artificial viscosity. Indeed, the artificial viscosity naturally increases the scheme stability and it turns out to be a suitable ingredient to establish the required entropy inequality (17). As a consequence, we here modify the numerical flux function $\mathcal{F}(w_L^+, w_R^-)$ by introducing

$$\mathcal{F}^{\gamma}_{LR} = \mathcal{F}(w_L^+, w_R^-) + \gamma \delta_{LR}, \tag{18}$$

where $\delta_{LR} = {}^t(\delta^h, \delta^q) \in \mathbb{R}^2$ stands for a nonlinear viscosity to be defined according to a correct control of the numerical entropy dissipation rate. The parameter $\gamma \geq 0$ governs the numerical artificial viscosity according to the CFL condition. In addition, in the above definition, w_L^+ and w_R^- stand for the reconstructed states at the interface according to (10). Put in other words, at an interface $x_{i+\frac{1}{2}}$, we set $w_L^+ = w^-_{i+\frac{1}{2}}$ and

$w_R^- = w_{i+\frac{1}{2}}^+$. Let us underline that this new numerical flux function definition depends on both reconstructed values and cell values; namely $\mathcal{F}_{LR}^\gamma := \mathcal{F}_{LR}^\gamma(w_L, w_R, w_L^+, w_R^-)$.

Now, instead of the numerical method (11), we consider the following scheme:

$$w_i^{n+1} = w_i^n - \frac{\Delta t}{\Delta x}\left(\mathcal{F}_{i+\frac{1}{2}}^\gamma - \mathcal{F}_{i-\frac{1}{2}}^\gamma\right) - g\Delta t \begin{pmatrix} 0 \\ \overline{h\partial_x z_i}^n \end{pmatrix}, \tag{19}$$

which reads

$$\begin{aligned} w_i^{n+1} = w_i^n - \frac{\Delta t}{\Delta x}\left(\mathcal{F}(w_{i+\frac{1}{2}}^-, w_{i+\frac{1}{2}}^+) - \mathcal{F}(w_{i-\frac{1}{2}}^-, w_{i-\frac{1}{2}}^+)\right) \\ + \gamma\frac{\Delta t}{\Delta x}\left(\delta_{i-\frac{1}{2}} - \delta_{i+\frac{1}{2}}\right) - g\Delta t \begin{pmatrix} 0 \\ \overline{h\partial_x z_i}^n \end{pmatrix}. \end{aligned} \tag{20}$$

For the sake of simplicity in the notations, adopting (13), we set

$$S_{i+\frac{1}{2}}^\pm = \begin{pmatrix} 0 \\ -g\overline{h\partial_x z}_{i+\frac{1}{2}}^\pm \end{pmatrix}, \tag{21}$$

to write, after (12),

$$-g \begin{pmatrix} 0 \\ \overline{h\partial_x z_i}^n \end{pmatrix} = S_{i-\frac{1}{2}}^+ + S_{i+\frac{1}{2}}^-.$$

From now on, it is worth noticing that the adopted scheme (20) needs a specific definition of δ_{LR} to recover the expected well-balanced property. Indeed, as soon as the sequence $(w_i^n)_{i\in\mathbb{Z}}$ defines a lake at rest at time t^n, because of the hydrostatic reconstruction conditions (15), we immediately obtain

$$w_i^{n+1} = w_i^n + \gamma\frac{\Delta t}{\Delta x}\left(\delta_{i-\frac{1}{2}} - \delta_{i+\frac{1}{2}}\right).$$

As a consequence, we have to impose $\delta_{LR} = 0$ as soon as w_L and w_R define a lake at rest. Moreover, in order to preserve the consistency property of (20), we must have $\delta_{i+\frac{1}{2}} - \delta_{i-\frac{1}{2}} = \mathcal{O}(\Delta x^2)$.

Now, in order to prove the energy estimation (17), we suggest to reformulate the viscous hydrostatic reconstruction scheme (20) as a Godunov-type method. To address such an issue, we introduce the following approximate Riemann solver:

$$w^{\mathcal{R}}\left(\frac{x}{t}; w_L, w_R, w_L^+, w_R^-\right) = \begin{cases} w_L & \text{if} \quad \dfrac{x}{t} < -(\lambda+\gamma), \\ \bar{w}_L & \text{if} \quad -(\lambda+\gamma) < \dfrac{x}{t} < -\lambda, \\ w_L^\star & \text{if} \quad -\lambda < \dfrac{x}{t} < 0, \\ w_R^\star & \text{if} \quad 0 < \dfrac{x}{t} < \lambda, \\ \bar{w}_R & \text{if} \quad \lambda < \dfrac{x}{t} < \lambda+\gamma, \\ w_R & \text{if} \quad \dfrac{x}{t} > \lambda+\gamma, \end{cases} \tag{22}$$

where we have set

$$\bar{w}_L = w_L - \delta_{LR} \quad \text{and} \quad \bar{w}_R = w_R + \delta_{LR} \tag{23}$$

and

$$\begin{aligned} w_L^\star &= w_L - \frac{1}{\lambda}\left(\mathcal{F}(w_L^+, w_R^-) - f(w_L)\right) + \frac{\Delta x}{\lambda}S_L^+, \\ w_R^\star &= w_R + \frac{1}{\lambda}\left(\mathcal{F}(w_L^+, w_R^-) - f(w_R)\right) + \frac{\Delta x}{\lambda}S_R^-. \end{aligned} \tag{24}$$

In the above definition, S_L^+ and S_R^- denote the source term discretization at the interface according to (21); namely $S_L^+ = S_{i+\frac{1}{2}}^-$ and $S_R^- = S_{i+\frac{1}{2}}^+$ at each side of the interface $x_{i+\frac{1}{2}}$.

Concerning the wave speeds involved in (22), $\lambda > 0$ and $\gamma \geq 0$ will be fixed later on according to stability conditions to be prescribed. For the sake of simplicity in the forthcoming developments, γ is fixed to a constant value over the whole mesh while λ is defined locally interface per interface.

Next, arguing direct computations, the updated state w_i^{n+1}, given by (20), equivalently reformulates as follows:

$$\begin{aligned} w_i^{n+1} =& \frac{1}{\Delta x} \int_0^{\frac{\Delta x}{2}} w^{\mathcal{R}} \left(\frac{x}{\Delta t}; w_{i-1}^n, w_i^n, w_{i-\frac{1}{2}}^-, w_{i-\frac{1}{2}}^+ \right) \, dx \\ &+ \frac{1}{\Delta x} \int_{-\frac{\Delta x}{2}}^0 w^{\mathcal{R}} \left(\frac{x}{\Delta t}; w_i^n, w_{i+1}^n, w_{i+\frac{1}{2}}^-, w_{i+\frac{1}{2}}^+ \right) \, dx, \end{aligned} \tag{25}$$

under a CFL-like condition given by

$$\frac{\Delta t}{\Delta x} \max_{i \in \mathbb{Z}} \left(\lambda_{i+\frac{1}{2}} + \gamma \right) \leq \frac{1}{2}. \tag{26}$$

We recall that this CFL restriction imposes non-interaction of successive approximate Riemann solvers

$$w^{\mathcal{R}} \left(\frac{x - x_{i-\frac{1}{2}}}{\Delta t}; w_{i-1}^n, w_i^n, w_{i-\frac{1}{2}}^-, w_{i-\frac{1}{2}}^+ \right) \text{ and } w^{\mathcal{R}} \left(\frac{x - x_{i+\frac{1}{2}}}{\Delta t}; w_i^n, w_{i+1}^n, w_{i+\frac{1}{2}}^-, w_{i+\frac{1}{2}}^+ \right).$$

To conclude this section, we underline that the initial hydrostatic reconstruction scheme (11) is recovered as soon as $\gamma = 0$.

3 Discrete entropy inequality

Equipped with the improved hydrostatic reconstruction scheme (20) and the associated Godunov-type reformulation (25), we are now able to get the expected discrete energy estimate (17). Indeed, involving the work by Harten, Lax and van Leer [27], the Godunov-type scheme (25) is entropy preserving as soon as the approximate Riemann solver (22) satisfies the following interface entropy condition:

$$\begin{aligned} &\frac{1}{\Delta x} \int_{-\frac{\Delta x}{2}}^{\frac{\Delta x}{2}} \tilde{\eta} \left(w^{\mathcal{R}} \left(\frac{x}{\Delta t}; w_L, w_R, w_L^+, w_R^- \right), z \right) \, dx \\ &\qquad \leq \frac{1}{2} \left(\tilde{\eta}(w_L, z_L) + \tilde{\eta}(w_R, z_R) \right) - \frac{\Delta t}{\Delta x} \left(\tilde{G}(w_R, z_R) - \tilde{G}(w_L, z_L) \right), \end{aligned} \tag{27}$$

with the entropy pair $(\tilde{\eta}, \tilde{G})$ defined by (5) and where we have set

$$z = \begin{cases} z_L & \text{if} \quad x < 0, \\ z_R & \text{if} \quad x > 0. \end{cases}$$

Indeed, since η, defined by (3), is a convex function, involving the well-known Jensen's inequality, we immediately obtain

$$\begin{aligned} \eta(w_i^{n+1}) \leq& \frac{1}{\Delta x} \int_0^{\frac{\Delta x}{2}} \eta \left(w^{\mathcal{R}} \left(\frac{x}{\Delta t}; w_{i-1}^n, w_i^n, w_{i-\frac{1}{2}}^-, w_{i-\frac{1}{2}}^+ \right) \right) \, dx \\ &+ \frac{1}{\Delta x} \int_{-\frac{\Delta x}{2}}^0 \eta \left(w^{\mathcal{R}} \left(\frac{x}{\Delta t}; w_i^n, w_{i+1}^n, w_{i+\frac{1}{2}}^-, w_{i+\frac{1}{2}}^+ \right) \right) \, dx. \end{aligned}$$

Moreover, we have

$$h_i^{n+1} z_i = \frac{1}{\Delta x} \int_0^{\frac{\Delta x}{2}} h^{\mathcal{R}} \left(\frac{x}{\Delta t}; w_{i-1}^n, w_i^n, w_{i-\frac{1}{2}}^-, w_{i-\frac{1}{2}}^+ \right) z_i \, dx + \frac{1}{\Delta x} \int_{-\frac{\Delta x}{2}}^0 h^{\mathcal{R}} \left(\frac{x}{\Delta t}; w_i^n, w_{i+1}^n, w_{i+\frac{1}{2}}^-, w_{i+\frac{1}{2}}^+ \right) z_i \, dx,$$

so that, adding the above identities, by definition of $\tilde{\eta}$ given by (5), we get

$$\tilde{\eta}(w_i^{n+1}, z_i) \leq \frac{1}{\Delta x} \int_0^{\frac{\Delta x}{2}} \tilde{\eta} \left(w^{\mathcal{R}} \left(\frac{x}{\Delta t}; w_{i-1}^n, w_i^n, w_{i-\frac{1}{2}}^-, w_{i-\frac{1}{2}}^+ \right), z_i \right) dx + \frac{1}{\Delta x} \int_{-\frac{\Delta x}{2}}^0 \tilde{\eta} \left(w^{\mathcal{R}} \left(\frac{x}{\Delta t}; w_i^n, w_{i+1}^n, w_{i+\frac{1}{2}}^-, w_{i+\frac{1}{2}}^+ \right), z_i \right) dx.$$

Next, arguing the inequality (27), a straightforward computation gives the expected entropy inequality (17) where the entropy numerical flux function is defined as follows:

$$\tilde{\mathcal{G}}(w_L, w_R, w_L^+, w_R^-, z_L, z_R) = \tilde{G}(w_R, z_R) - \frac{\Delta x}{2\Delta t} \tilde{\eta}(w_R, z_R) + \frac{1}{\Delta t} \int_0^{\frac{\Delta x}{2}} \tilde{\eta} \left(w^{\mathcal{R}} \left(\frac{x}{\Delta t}; w_L, w_R, w_L^+, w_R^- \right), z_R \right) dx.$$

As a consequence, we have now to establish the interface entropy inequality (27). To obtain this estimation, we first introduce the following entropy dissipation rate:

$$\mathcal{E} = \frac{1}{\Delta t} \int_{-\frac{\Delta x}{2}}^{\frac{\Delta x}{2}} \tilde{\eta} \left(w^{\mathcal{R}} \left(\frac{x}{\Delta t}; w_L, w_R, w_L^+, w_R^- \right), z \right) dx - \frac{\Delta x}{2\Delta t} \left(\tilde{\eta}(w_L, z_L) + \tilde{\eta}(w_R, z_R) \right) + \left(\tilde{G}(w_R, z_R) - \tilde{G}(w_L, z_L) \right), \tag{28}$$

so that the estimation (27) immediately reformulates as $\mathcal{E} \leq 0$. Next, from (22) to define the approximate Riemann solver, a straightforward computation gives:

$$\mathcal{E} = \mathcal{E}_0 + \gamma \mathcal{D},$$

where we have set

$$\mathcal{E}_0 = \lambda \Big(\tilde{\eta}(w_L^\star, z_L) + \tilde{\eta}(w_R^\star, z_R) - \tilde{\eta}(w_L, z_L) - \tilde{\eta}(w_R, z_R) \Big) + \left(\tilde{G}(w_R, z_R) - \tilde{G}(w_L, z_L) \right), \tag{29}$$

$$\mathcal{D} = \tilde{\eta}(\bar{w}_L, z_L) + \tilde{\eta}(\bar{w}_R, z_R) - \tilde{\eta}(w_L, z_L) - \tilde{\eta}(w_R, z_R). \tag{30}$$

We notice that $\mathcal{E}_0$ is nothing but the entropy dissipation rate of the initial hydrostatic reconstruction scheme (11), obtained by imposing $\gamma = 0$ in (20). The quantity $\mathcal{D}$ coincides with a viscous entropy dissipation rate associated with the artificial viscosity.

In fact, since the initial hydrostatic reconstruction scheme is not necessarily entropy preserving, the associated entropy dissipation rate $\mathcal{E}_0$ may be positive. As a consequence, we may have $\mathcal{E}_0 \geq 0$. Then, in order to recover $\mathcal{E} \leq 0$, necessarily we must have $\mathcal{D} < 0$ so that, with large enough value of $\gamma \geq 0$, we may expect a negative entropy dissipation $\mathcal{E}$. In fact, choosing the artificial viscosity as follows (for instance, see [12]):

$$\delta^h = \frac{1}{2}(h_L - h_R) \quad \text{and} \quad \delta^q = \frac{1}{2}(h_L u_L - h_R u_R),$$

we obtain

$$\bar{w}_L = \bar{w}_R = \frac{1}{2}(w_L + w_R).$$

With a flat topography, $z_L = z_R$, arguing the convexity of η, we immediately obtain $\mathcal{D} \leq 0$. Now, we have to extend such a viscosity definition in order to deal with non-flat topography.

Lemma 3.1. *Let w_L and w_R be two constant states in Ω_0. Assume the artificial viscosity δ_{LR} be given as follows:*

$$\delta^h = \frac{1}{2}(h_L - h_R) + \frac{1}{2}(z_L - z_R), \tag{31}$$

$$\delta^q = \frac{1}{2}(h_L u_L - h_R u_R) - \frac{1}{2}\frac{h_L u_L + h_R u_R}{h_L + h_R}(z_R - z_L). \tag{32}$$

Then the viscous entropy dissipation rate $\mathcal{D}$ reads

$$\mathcal{D} = -g(\delta^h)^2 - \frac{1}{2}\frac{h_L h_R}{h_L + h_R}(u_L - u_R)^2. \tag{33}$$

Assume the interface topography reconstruction $z_{LR}^- = z_{LR}^+ = z_{LR}$ be defined such that

$$z_{LR} = \frac{1}{2}(z_L + z_R) + \lambda K u (z_R - z_L), \tag{34}$$

as soon as $u_L = u_R = u$ and $h_L + z_L = h_R + z_R = H$ for given constants u and H. Moreover, in (34), λ is the wave speed involved in (22) and K is a parameter such that

$$0 < K u^2 < 1. \tag{35}$$

In addition, assume h_L and h_R be large enough such that

$$\frac{1}{2}(h_L + h_R) \pm \frac{1}{2}(z_R - z_L) > 0, \tag{36}$$

$$h_L + z_L - z_{LR} > 0 \quad \text{and} \quad h_R + z_R - z_{LR} > 0. \tag{37}$$

Then there exists $\lambda > 0$ and $\gamma \geq 0$ large enough such that the interface entropy inequality (27) is satisfied.

From now on, we underline that the condition (36) enforces the intermediate water heights $\bar{h}_L$ and $\bar{h}_R$ to be positive. Indeed, by definition of δ^h, now given by (31), we easily get

$$\bar{h}_L = \frac{1}{2}(h_L + h_R) - \frac{1}{2}(z_L - z_R) \quad \text{and} \quad \bar{h}_R = \frac{1}{2}(h_L + h_R) + \frac{1}{2}(z_L - z_R).$$

As a consequence, as long as the solution stays far away from dry areas, with $h_L \geq h_0 > 0$ and $h_R \geq h_0 > 0$, and with a smooth topography function, both $\bar{h}_L$ and $\bar{h}_R$ remain positive for small enough Δx. Moreover, the condition (37) imposes that the reconstructed water heights h_L^- and h_R^+ remain positive. As a consequence, at the level of the scheme presentation, we assume to be far away from dry areas. In the next section, extensions of the interface topography z_{LR} are proposed in order to deal with wet and dry transitions.

In addition, it is worth noticing that the proposed improved hydrostatic scheme is now defined up to the parameter K, involved in (34). The behavior of the approximated solution according to this parameter K will be numerically studied.

Moreover, at this level, we are not able to establish that λ and γ are bounded. However, in Section 4, devoted to the numerical experiments, we will illustrate the good behavior of these two parameters.

Proof. Arguing the definition of δ^h and δ^q, given by (31) and (32), after a laborious but straightforward computation, $\mathcal{D}$ is now given by (33). As a consequence, $\mathcal{D} \leq 0$ with equality to zero if and only if (w_L, z_L) and (w_R, z_R) belong to

$$\Gamma_{(H,u)} = \{h_L + z_L = h_R + z_R = H \text{ and } u_L = u_R = u\}.$$

Moreover, we notice that $\mathcal{D}$ and $\mathcal{E}_0$ do not depend on γ. Then, as long as $\mathcal{D} < 0$, there exists $\gamma \geq 0$ such that $\mathcal{E}_0 + \gamma\mathcal{D} \leq 0$.

Next, let us assume that (w_L, z_L) and (w_R, z_R) stay in $\Gamma_{(H,u)}$ so that $\mathcal{D} = 0$. In order to obtain the required inequality (27), we have now to establish that $\mathcal{E}_0 \leq 0$. By definition of the hydrostatic reconstruction (15), since $h_L + z_L = h_R + z_R$ and $u_L = u_R$, we have $w_L^+ = w_R^-$ where

$$h_L^+ = H - z_{LR} = h_R^-.$$

Now, we are able to evaluate both intermediate states $w_L^\star$ and $w_R^\star$ given by (24). Concerning the intermediate water heights, we have the following sequence of equalities:

$$h_L^\star = h_L - \frac{1}{\lambda}\left(h_L^+ u - h_L u\right) = h_L - \frac{u}{\lambda}\left(z_L - z_{LR})\right),$$
$$h_R^\star = h_R + \frac{1}{\lambda}\left(h_R^- u - h_R u\right) = h_R + \frac{u}{\lambda}\left(z_R - z_{LR})\right).$$

Next, concerning the intermediate discharge, we have

$$h_L^\star u_L^\star = h_L u_L - \frac{1}{\lambda}\left(f^{hu}(w_L^+) - f^{hu}(w_L)\right) + \frac{g}{2\lambda}\left((h_L^+)^2 - h_L^2\right),$$
$$h_R^\star u_R^\star = h_R u_R + \frac{1}{\lambda}\left(f^{hu}(w_R^-) - f^{hu}(w_R)\right) + \frac{g}{2\lambda}\left(h_R^2 - (h_R^-)^2\right),$$

to get

$$h_L^\star u_L^\star = h_L u - \frac{u^2}{\lambda}(z_L - z_{LR}),$$
$$h_R^\star u_R^\star = h_R u + \frac{u^2}{\lambda}(z_R - z_{LR}).$$

Plugging these intermediate states within $\mathcal{E}_0$ and adopting an interface topography z_{LR} given by (34), after a huge but direct computation, we obtain

$$\mathcal{E}_0 = u^2 K g (z_R - z_L)^2 (K u^2 - 1)\lambda^2 + \alpha_1 \lambda + \alpha_0,$$

where α_1 and α_0 do not depend on λ. As a consequence, as long as $u \neq 0$ and $z_L \neq z_R$, under the condition (35), $\mathcal{E}_0$ stands for a second-order polynomial function with respect to λ with a negative head coefficient. Hence, there exists $\lambda > 0$ large enough such that $\mathcal{E}_0 < 0$.

Finally, to conclude the proof, we underline that $\Gamma_{(H,0)}$ coincides with the lake at rest. Then, by definition of the hydrostatic reconstruction (15), we immediately obtain $w_L^\star = w_L$ and $w_R^\star = w_R$ so that $\mathcal{E}_0 = 0$ to get $\mathcal{E} = 0$. Moreover, if we restrict $\Gamma_{(H,u)}$ to $z_L = z_R$, then we enforce $w_L = w_R$. By definition of the entropy dissipation rate, once again we obtain $\mathcal{E} = 0$. The proof is thus completed. □

We now conclude this section by stating our main result.

Theorem 3.1. *Let $\mathcal{F}(w_L, w_R)$ be a consistent numerical flux function with the homogeneous shallow-water equations. Assume the topography function z be given by a smooth function. Let $(w_i^n)_{i\in\mathbb{Z}}$ be a sequence in Ω_0 to approximate the solution of (1) at time t^n. Consider the updated state w_i^{n+1} given by the viscous hydrostatic reconstruction scheme (20) and (13) where the reconstructed water heights are given by (9) but for an interface topography defined by*

$$z_{i+\frac{1}{2}}^- = z_{i+\frac{1}{2}}^+ = z_{i+\frac{1}{2}}, \tag{38}$$
$$z_{i+\frac{1}{2}} = \frac{1}{2}(z_i + z_{i+1}) + \frac{\lambda}{2}(u_i^n + u_{i+1}^n)(z_{i+1} - z_i)K_{i+\frac{1}{2}}, \tag{39}$$

with $K_{i+\frac{1}{2}}$ a positive parameter such that

$$0 < \frac{K_{i+\frac{1}{2}}}{4}\left((u_i^n)^2 + (u_{i+1}^n)^2\right) < 1.$$

Concerning the artificial viscosity $\delta_{i+\frac{1}{2}} = {}^t(\delta^h_{i+\frac{1}{2}}, \delta^q_{i+\frac{1}{2}})$, *we adopt*

$$\delta^h_{i+\frac{1}{2}} = \frac{1}{2}(h^n_i - h^n_{i+1}) + \frac{1}{2}(z_i - z_{i+1}), \tag{40}$$

$$\delta^q_{i+\frac{1}{2}} = \frac{1}{2}(h^n_i u^n_i - h^n_{i+1}u^n_{i+1}) - \frac{1}{2}\frac{h^n_i u^n_i + h^n_{i+1}u^n_{i+1}}{h^n_i + h^n_{i+1}}(z_{i+1} - z_i). \tag{41}$$

Under the CFL-like restriction (26), there exists $\lambda_{i+\frac{1}{2}} > 0$ *and* $\gamma \geq 0$ *large enough such that the scheme is*

(i) consistent,

(ii) well-balanced for the lake at rest,

(iii) entropy preserving according to the discrete energy estimate (17).

It is worth noticing that no stability conditions are imposed to be satisfied by the numerical flux function $\mathcal{F}$. In fact, all the required stability is contained within the numerical artificial viscosity.

Proof. First, let us show that the scheme is consistent. Since the topography function is smooth, we immediately have the consistency of the interface topography $z_{i+\frac{1}{2}}$ up to $\mathcal{O}(\Delta x)$. As a consequence, the reconstruction states $w^{\pm}_{i+\frac{1}{2}}$ are consistent up to $\mathcal{O}(\Delta x)$. Then, $(\mathcal{F}(w^-_{i+\frac{1}{2}}, w^+_{i+\frac{1}{2}}) - \mathcal{F}(w^+_{i-\frac{1}{2}}, w^+_{i-\frac{1}{2}}))/\Delta x$ is naturally consistent with $\partial_x f(w)$ up to $\mathcal{O}(\Delta x)$. Next, concerning the artificial viscosity, we have

$$\begin{aligned}
\delta^h_{i-\frac{1}{2}} - \delta^h_{i+\frac{1}{2}} &= \frac{1}{2}(h^n_{i+1} - 2h^n_i + h^n_{i-1}) + \frac{1}{2}(z_{i+1} - 2z_i + z_{i-1}),\\
\delta^q_{i-\frac{1}{2}} - \delta^q_{i+\frac{1}{2}} &= \frac{1}{2}((hu)^n_{i+1} - 2(hu)^n_i + (hu)^n_{i-1})\\
&\quad - \frac{1}{2}\left(\frac{(hu)^n_i + (hu)^n_{i+1}}{h^n_i + h^n_{i+1}}(z_{i+1} - z_i) - \frac{(hu)^n_{i-1} + (hu)^n_i}{h^n_{i-1} + h^n_i}(z_i - z_{i-1})\right),
\end{aligned}$$

to immediately obtain $\delta^h_{i+\frac{1}{2}} - \delta^h_{i-\frac{1}{2}} = \mathcal{O}(\Delta x^2)$ and $\delta^q_{i+\frac{1}{2}} - \delta^q_{i-\frac{1}{2}} = \mathcal{O}(\Delta x^2)$. As a consequence, the artificial viscosity is consistent with zero. Concerning the source term, the consistency is immediately recovered because of the consistency of the interface topography $z_{i+\frac{1}{2}}$.

Next, concerning the well-balanced property, since $z^-_{i+\frac{1}{2}} = z^+_{i+\frac{1}{2}} = z_{i+\frac{1}{2}}$, we have just to show that the artificial viscosity vanishes as soon as a lake at rest is considered. But, as soon as $h^n_i + z_i = h^n_{i+1} + z_{i+1}$, we get $\delta^h_{i+\frac{1}{2}} = 0$. Moreover, with $\delta^h_{i+\frac{1}{2}} = 0$, we have $\delta^q_{i+\frac{1}{2}} = 0$ with $u^n_i = u^n_{i+1} = 0$. Then, the considered scheme is well-balanced.

Finally, the discrete entropy inequality (17) is a direct consequence of Lemma 3.1. The proof is thus achieved. □

4 Wet and dry transitions

We underline that, in the work by Audusse et al [1] (see also [11, 38]), the hydrostatic reconstruction scheme remains relevant when considering wet and dry transitions. More precisely, the hydrostatic reconstruction technique preserves the water height nonnegative. Such a property is essential to perform numerical simulations of physical interest. Here, we propose to modify the water height reconstructions and the artificial viscosity in order to make relevant the derived numerical scheme within dry areas.

Concerning the water height reconstructions, we adopt the approach introduced by Audusse et al [1], by imposing on the cell $(x_{i-\frac{1}{2}}, x_{i+\frac{1}{2}})$, $h^+_{i-\frac{1}{2}} \geq 0$ and $h^-_{i+\frac{1}{2}} \geq 0$ but also $h^+_{i-\frac{1}{2}} = h^-_{i+\frac{1}{2}} = 0$ if $h^n_i = 0$. To address such an issue, we suggest

$$
\begin{aligned}
h^+_{i-\frac{1}{2}} &= \max\left(0, h^n_i + \alpha^+_{i-\frac{1}{2}}(z_i - z_{i-\frac{1}{2}})\right), \\
h^-_{i+\frac{1}{2}} &= \max\left(0, h^n_i + \alpha^-_{i+\frac{1}{2}}(z_i - z_{i+\frac{1}{2}})\right),
\end{aligned}
$$

with $z_{i+\frac{1}{2}}$ given by (39) and where we have set

$$
\begin{aligned}
\alpha^+_{i-\frac{1}{2}} &= \frac{h^n_i}{h^n_i + \left(|h^n_i + z_i - h^n_{i-1} - z_{i-1}| + |u^n_i - u^n_{i-1}|\right)\Delta x^k}, \\
\alpha^-_{i+\frac{1}{2}} &= \frac{h^n_i}{h^n_i + \left(|h^n_{i+1} + z_{i+1} - h^n_i - z_i| + |u^n_{i+1} - u^n_i|\right)\Delta x^k},
\end{aligned}
$$

for a given $k \geq 1$.

Adopting the notations introduced in (9), we get

$$
h^+_{i-\frac{1}{2}} = h^n_i + z_i - z^+_{i-\frac{1}{2}} \quad \text{and} \quad h^-_{i+\frac{1}{2}} = h^n_i + z_i - z^-_{i+\frac{1}{2}}, \tag{42}
$$

where we have set

$$
\begin{aligned}
z^-_{i+\frac{1}{2}} &= \min\left(h^n_i + z_i, z_i - \alpha^-_{i+\frac{1}{2}}(z_i - z_{i+\frac{1}{2}})\right), \\
z^+_{i-\frac{1}{2}} &= \min\left(h^n_i + z_i, z_i - \alpha^+_{i-\frac{1}{2}}(z_i - z_{i-\frac{1}{2}})\right).
\end{aligned} \tag{43}
$$

Next, let us focus on the artificial viscosity. We suggest to consider a similar cut-off technique by imposing the water height artificial viscosity $\delta^h_{i+\frac{1}{2}}$ such that $h^n_i - \delta^h_{i+\frac{1}{2}} \geq 0$ and $h^n_{i+1} + \delta^h_{i+\frac{1}{2}} \geq 0$. As a consequence, we propose

$$
\delta^h_{i+\frac{1}{2}} = \max\left(-h^n_{i+1}, \min\left(h^n_i, \frac{1}{2}(h^n_i + z^n_i - h^n_{i+1} - z_{i+1})\right)\right). \tag{44}
$$

In addition, in order to preserve the water heights nonnegative, as usual, we impose that the adopted numerical flux function $\mathcal{F}(w_L, w_R)$ is associated with a nonnegative preserving scheme over a flat topography (for instance, see [1, 11]). Put in other words, we impose that

$$
\mathcal{F}^h(w = 0, w^n_{i+1}) - \mathcal{F}^h(w^n_{i-1}, w = 0) \leq 0, \tag{45}
$$

for all states $w^n_{i\pm1}$ in Ω.

We now show that the resulting scheme is nonnegative preserving and it preserves the stability property established Theorem 3.1.

Theorem 4.1. *Let $(w^n_i)_{i\in\mathbb{Z}}$ be given in Ω. Consider the viscous hydrostatic reconstruction scheme (20) and (13) with reconstructed water heights given by (42) and (43), and an artificial viscosity defined by (41) and (44).*

(i) The scheme is consistent.

(ii) The scheme is well-balanced; namely if $h^n_i + z_i = H$ and $u^n_i = 0$ for all i in $\mathbb{Z}$, then $h^{n+1}_i + z_i = H$ and $u^{n+1}_i = 0$ for all i in $\mathbb{Z}$.

(iii) Up to a more restrictive CFL-like condition, the scheme is nonnegative preserving; namely if $h^n_i \geq 0$ for all i in $\mathbb{Z}$, then $h^{n+1}_i \geq 0$ for all i in $\mathbb{Z}$.

(iv) The scheme is entropy preserving according to the discrete entropy inequality (17) in Ω_0 at least for small enough Δx.

Proof. Concerning the consistency of the scheme, it easily comes from the consistency of $z^{\pm}_{i+\frac{1}{2}}$ with the topography function z. We notice that $z_{i+\frac{1}{2}}$, defined by (39), is consistent with z while $\alpha^{\pm}_{i+\frac{1}{2}}$ is consistent with 1. As a consequence, $z^{\pm}_{i+\frac{1}{2}}$ is consistent with $\min(h+z,z)=z$ and the considered scheme is proved to be consistent.

Next, in order to prove (ii), let us consider a lake at rest; namely $h_i^n + z_i = H$ and $u_i^n = 0$ for all i in $\mathbb{Z}$. Arguing (41) and (44), we immediately get

$$\delta^h_{i+\frac{1}{2}} = 0 \quad \text{and} \quad \delta^q_{i+\frac{1}{2}} = 0.$$

Moreover, we get $\alpha^{\pm}_{i+\frac{1}{2}} = 1$. With the definition of the interface topography, given by (43), we have

$$z^{\pm}_{i+\frac{1}{2}} = \min(H, z_{i+\frac{1}{2}}),$$

so that $h^-_{i+\frac{1}{2}} = h^+_{i+\frac{1}{2}}$. Since $u_i^n = 0$ for all i in $\mathbb{Z}$, the numerical flux function reads for all i in $\mathbb{Z}$

$$\mathcal{F}(w^-_{i+\frac{1}{2}}, w^+_{i+\frac{1}{2}}) = f\begin{pmatrix} h^-_{i+\frac{1}{2}} \\ 0 \end{pmatrix} = \begin{pmatrix} 0 \\ \dfrac{g}{2}(h^-_{i+\frac{1}{2}})^2 \end{pmatrix}.$$

After a direct computation, the scheme (20) now gives $w_i^{n+1} = w_i^n$ and the well-balanced property is stated.

Next, we turn establishing (iii). To address such an issue, we introduce the following two partial updated water heights:

$$\begin{aligned} h_i^{n+1,1} &= h_i^n - \frac{\Delta t}{\Delta x/2}\left(\mathcal{F}^h(w^-_{i+\frac{1}{2}}, w^+_{i+\frac{1}{2}}) - \mathcal{F}^h(w^-_{i-\frac{1}{2}}, w^+_{i-\frac{1}{2}})\right), \\ h_i^{n+1,2} &= h_i^n + \gamma\frac{\Delta t}{\Delta x/2}\left(\delta^h_{i-\frac{1}{2}} - \delta^h_{i+\frac{1}{2}}\right), \end{aligned}$$

such that the updated water height defined by (20) now reformulates as follows:

$$h_i^{n+1} = \frac{1}{2}\left(h_i^{n+1,1} + h_i^{n+1,2}\right). \tag{46}$$

We recognize $h_i^{n+1,1}$ as the updated state given by a hydrostatic reconstruction scheme according to the work by Audusse et al [1]. Since $h^+_{i-\frac{1}{2}} = h^-_{i+\frac{1}{2}} = 0$ as soon as $h_i^n = 0$, the nonnegative condition (45) to be satisfied by the numerical flux function implies $h_i^{n+1} \geq 0$ (see [1, 11] for more detail), under the CFL-like condition

$$\frac{\Delta t}{\Delta x/2}\max_{i\in\mathbb{Z}}\lambda_{i+\frac{1}{2}} \leq \frac{1}{2}.$$

Next, concerning $h_i^{n+1,2}$, after a straightforward computation we get

$$h_i^{n+1,2} = \left(1 - 4\frac{\Delta t}{\Delta x}\right)h_i^n + 2\frac{\Delta t}{\Delta x}(h_i^n + \delta^h_{i-\frac{1}{2}}) + 2\frac{\Delta t}{\Delta x}(h_i^n - \delta^h_{i+\frac{1}{2}}).$$

According to the definition of $\delta^h_{i+\frac{1}{2}}$, given by (44), we have $h_i^n - \delta^h_{i-\frac{1}{2}} \geq 0$ and $h_i^n + \delta^h_{i+\frac{1}{2}} \geq 0$. As a consequence, under the CFL-like condition

$$\frac{\Delta t}{\Delta x} \leq \frac{1}{4},$$

we get $h_i^{n+1,2} \geq 0$, to immediately obtain $h_i^{n+1} \geq 0$ according to (46).

To conclude the proof, we have to establish the discrete entropy inequality (17). In fact, it suffices to apply Lemma 3.1 for the new definition of the interface topography given by (43) and the new artificial viscosity (44). Since this stability property is considered in Ω_0, with Δx small enough, the viscosity $\delta^h_{i+\frac{1}{2}}$ recovers the expected formulation given by (40). Next, we notice that $\alpha^{\pm}_{i+\frac{1}{2}} = 1$ as soon as $h^n_i + z^n_i = h^n_{i+1} + z_{i+1} = H$ and $u^n_i = u^n_{i+1}$. As a consequence, with Δx small enough, in Ω_0 we get

$$z^{\pm}_{i+\frac{1}{2}} = \min(H, z_{i+\frac{1}{2}}) = z_{i+\frac{1}{2}},$$

and thus the condition (34) is satisfied and Lemma 3.1 can be applied. The proof is thus achieved. □

5 Numerical experiments

In this section, we display several numerical experiments to illustrate the relevance of the derived viscous hydrostatic reconstruction scheme (20) and (13) with the water height reconstruction given by (42) and (43), and the artificial viscosity given by (41) and (44).

The numerical simulations are performed involving two distinct numerical flux functions. First, we adopt the numerical flux function for the Suliciu relaxation scheme [7] or equivalently the HLLC scheme [46]. From now on, we emphasize that this scheme is entropy preserving for flat topography. Next, the second numerical flux function we adopt is associated with the VF-Roe scheme [16,17,35]. This second considered scheme is well-known to be entropy violating. As a consequence, wrong shock discontinuities may appear in the approximated solutions. Such a failure is very interesting to be tested within our stabilisation technique.

To implement the scheme, we have to specify the parameters. Concerning $\lambda_{i+\frac{1}{2}}$, in order to be consistent with the entropy inequality satisfied by the Suliciu relaxation scheme, we adopt

$$\lambda_{i+\frac{1}{2}} = \left(1 + \frac{1}{10}\right) \max_{i\in\mathbb{Z}} \left(|u^n_i| + \sqrt{g h^n_i}\right). \tag{47}$$

Concerning $K_{i+\frac{1}{2}}$, involved in $z_{i+\frac{1}{2}}$, and k, involved in $\alpha^{\pm}_{i+\frac{1}{2}}$, we fix this parameters as follows:

$$K_{i+\frac{1}{2}} = \min\left(\Delta x^2, \left(\frac{2}{(u^n_i)^2 + (u^n_{i+1})^2}\right)\right) \quad \text{and} \quad k = 2. \tag{48}$$

The influence of these parameters is tested later on.

Now, the main difficulty comes from the evaluation of γ to govern the artificial viscosity. In the simulations, we have decided to select one value of γ per time iteration. At time t^n, at each interface $x_{i+\frac{1}{2}}$, we evaluate $(\mathcal{E}_0)^n_{i+\frac{1}{2}}$ and $\mathcal{D}^n_{i+\frac{1}{2}}$, given by (29) and (30). Then, we fix γ^n such that $(\mathcal{E}_0)^n_{i+\frac{1}{2}} + \gamma^n \mathcal{D}^n_{i+\frac{1}{2}} \leq 0$.

Equipped with the values of $\lambda_{i+\frac{1}{2}}$ and γ^n, the time increment Δt^n is evaluated at each time iteration according to the CFL-like restriction (26) as follows:

$$\Delta t^n = \frac{\Delta x}{2 \max\limits_{i\in\mathbb{Z}} \left(\lambda_{i+\frac{1}{2}} + \gamma\right)}. \tag{49}$$

In the sequel, we present three sequences of numerical experiments respectively devoted to dam-breaks over a flat topography, stationary flows over a bump and wet/dry transitions.

5.1 Dam-breaks over a flat topography

Here, the simulation domain is made of the interval $[0, 25]$ where the topography function is fixed to $z(x) = 0$. The initial data for the first dam-break is given by

$$h(x,0) = \begin{cases} 1.5 & \text{if} \quad x < 12.5, \\ 0.5 & \text{if} \quad x > 12.5, \end{cases} \qquad \text{and} \qquad u(x,0) = 0. \tag{50}$$

The exact solution is made of a rarefaction wave and a shock wave. Since the Suliciu relaxation scheme is entropy preserving over a flat topography, the evaluation of the viscosity parameter imposes $\gamma^n = 0$ for all $n > 0$ in this simulation. Concerning the approximation given by the VF-Roe scheme, we also obtain $\gamma^n = 0$ for all $n > 0$. In fact, for such a Riemann problem, the VF-Roe scheme does not involve entropy fix and we obtain the expected approximate solution. The numerical results for this first dam-break are displayed Figure 2.

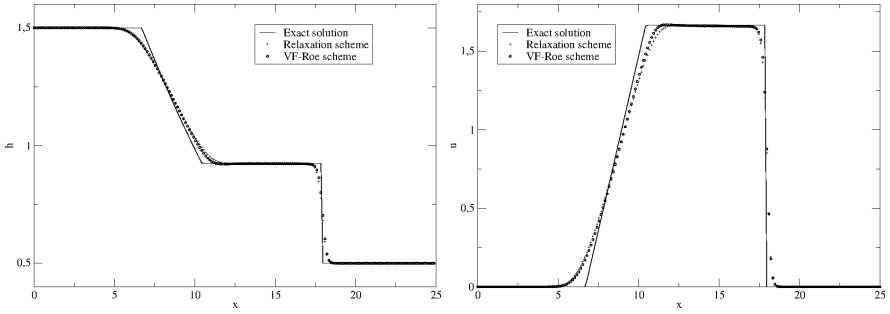

Figure 2: Numerical simulation obtained for the first dam-break given for the initial data (50) at time $t = 1.5$ with 200 cells.

The second simulated dam-break is obtained by considering the following initial data:

$$h(x,0) = \begin{cases} 2.0 & \text{if} \quad x < 12.5, \\ 0.1 & \text{if} \quad x > 12.5, \end{cases} \qquad \text{and} \qquad u(x,0) = 0. \tag{51}$$

Once again, the Suliciu relaxation scheme is entropy preserving and we obtain a good approximation of the solution made of a rarefaction wave and a shock wave. Now, the situation turns out to be drastically different concerning the VF-Roe scheme. Indeed, the VF-Roe scheme produces a strong entropy violating shock wave as displayed Figure 3.

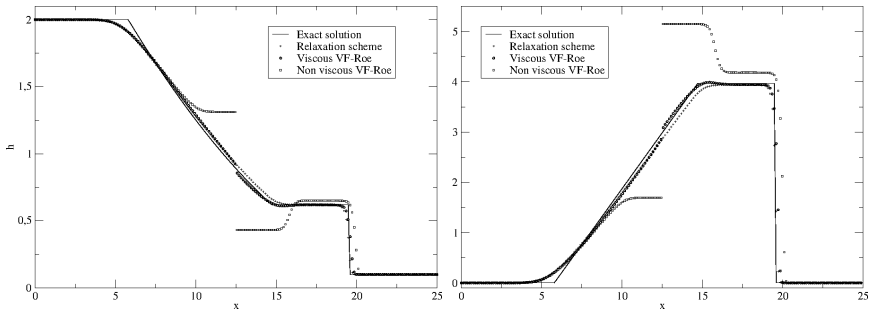

Figure 3: Numerical simulation obtained for the second dam-break given for the initial data (51) at time $t = 1.5$ with 200 cells.

Nevertheless, as soon as the artificial viscosity is activated, the entropy stability is recovered and the approximated solution becomes in a good agreement when compared to the exact solution.

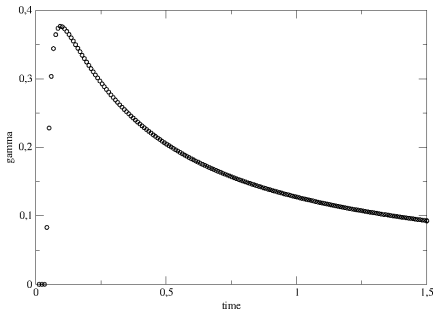

Figure 4: Second dam-break given for the initial data (51) at time $t = 1.5$ with 200 cells, evolution of the viscous parameter γ^n versus time.

Cells	L^2 water height error	L^2 discharge error
200	1.6197E-2	4.8550E-2
400	9.1830E-3	2.7253E-2
800	5.4305E-3	1.6455E-2
1600	3.0831E-3	8.8137E-3

Table 1: Errors evaluation of viscous VF-Roe scheme for the second dam-break with initial data (51).

In Figure 4, we present the evolution of γ^n versus time obtained during the simulation. It is clear that the values of γ^n do not restrict the CFL condition and do not perturb the order of accuracy as presented Table 1.

5.2 Stationary solutions

Now, we focus on simulations of stationary solutions. Here, the domain of simulation is given by $[0, 25]$ while the topography contains a bump as follows:

$$z(x) = \max(0, 0.2 - 0.05(x - 10)^2). \tag{52}$$

First, we simulate the well-known lake at rest. Then, the initial data is given by

$$h(x, 0) = \max(0, 0.5 - z(x)) \quad \text{and} \quad u(x, 0) = 0. \tag{53}$$

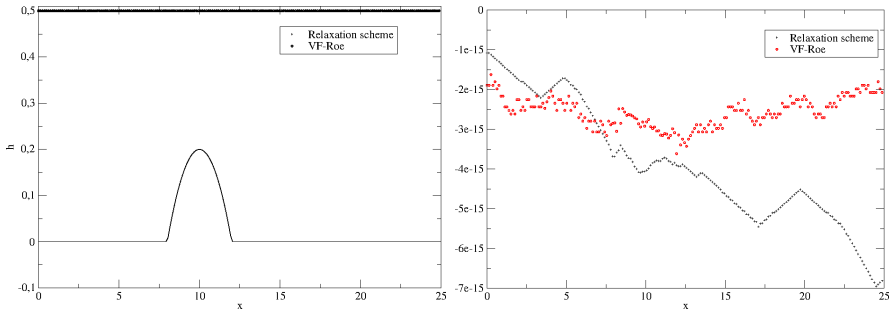

Figure 5: Numerical simulation obtained for the lake at rest given for the initial data (53) at time $t = 100$ with 200 cells.

As presented Figure 5, since the scheme is well-balanced, the initial data is preserved by both Suliciu scheme and VF-Roe scheme with errors equal to $\mathcal{O}(10^{-15})$. Of course, since the steady solution is exactly captured, the artificial viscosity remains equal to zero during the simulation.

Next, the second simulation is devoted to a subcritical flow with an initial data given by

$$h(x,0) = 2 - z(x) \quad \text{and} \quad u(x,0) = 0. \tag{54}$$

In this simulation, the boundary conditions are imposed as follows:

$$h(0,t)u(0,t) = h(25,t)u(25,t) = 4.42 \quad \text{and} \quad h(25,t) = 2$$

while $h(0,t)$ is given by an usual Newman condition.

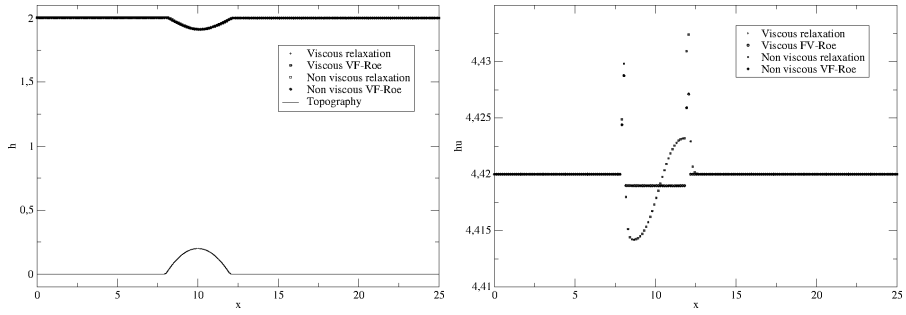

Figure 6: Numerical simulation obtained for the subcritical flow at time $t = 100$ with 200 cells.

The obtained numerical results are displayed Figure 6. Here, we present the results obtained by adopting the original version of the Suliciu relaxation scheme and the VF-Roe scheme as well as the viscous extension according to the introduced artificial viscosity technique. The discharge error evaluations, given Table 2 and Table 3, are clearly convincing. Because of the non vanishing topography function, the artificial viscosity is here active.

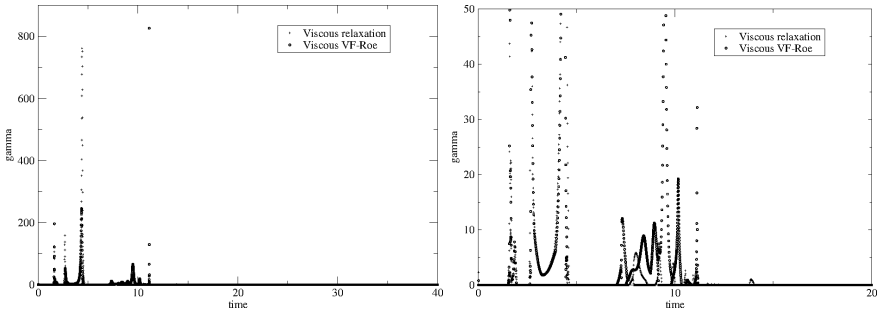

Figure 7: Evolution of γ^n versus time (left) and a zoom (right) obtained for the subcritical flow at time $t = 100$ with 200 cells.

In Figure 7, we display the obtained values of γ^n versus time. We notice that some values of γ^n are very large. However, these large values are only for some time iterations and not during all the simulation. As a consequence, it seems more relevant to introduce the time average of γ^n as follows:

$$\bar{\gamma} = \frac{1}{T} \sum_{n=0}^{N} \gamma^n \Delta t^n, \tag{55}$$

where N is the total number of time iteration performed by the simulation and T is the final time of the simulation.

In fact, once again, the artificial viscosity does not seem to impose a restrictive CFL condition. Such an assertion is confirmed in both Table 2 and Table 3 when exhibiting how much the artificial viscosity increases the number of time iterations. In addition, we

Cells	Non viscous relaxation			Viscous relaxation			
	L^2-error	$max(\mathcal{E}_0)$	N	L^2-error	$\max_{n>0}\gamma^n$	$\bar{\gamma}$	N (increase)
200	7.0821E-4	5.6105	11899	7.0822E-4	761.51	0.1055	12057 (1%)
400	3.0611E-4	5.6105	23883	3.0611E-4	839.24	0.1606	24377 (2%)
800	1.4219E-4	5.6105	47863	1.4218E-4	2089.60	0.3018	49745 (3%)
1600	6.8524E-5	5.6105	95843	6.8517E-5	197463.81	0.4054	100921 (5%)

Table 2: Subcritical flow at time $t = 100$ with the relaxation scheme. Evolution with respect to the cell number of the discharge L^2-error, the dissipation rate $\mathcal{E}_0$, the number of time iterations N and the percent increasing, the maximum value of γ^n and the average in time of γ^n.

Cells	Non viscous VF-Roe			Viscous VF-Roe			
	L^2-error	$max(\mathcal{E}_0)$	N	L^2-error	$\max_{n>0}\gamma^n$	$\bar{\gamma}$	N (increase)
200	2.8502E-4	1.9294	11880	2.8502E-4	825.92	0.2213	12231 (3%)
400	7.3086E-5	1.9294	23826	7.3086E-5	526.77	0.6017	25744 (8%)
800	1.8496E-5	1.9294	47718	1.8496E-5	2809.42	0.1962	48970 (2%)
1600	4.6518E-6	1.9294	95504	4.6518E-6	23790.89	0.2119	98214 (3%)

Table 3: Subcritical flow at time $t = 100$ with the VF-Roe scheme. Evolution with respect to the cell number of the discharge L^2-error, the dissipation rate $\mathcal{E}_0$, the number of time iterations N and the percent increasing, the maximum value of γ^n and the average in time of γ^n.

notice that the artificial viscosity does not modify the numerical error. Moreover, let us emphasize that the non viscous schemes violate the entropy condition since the entropy dissipation rate $\mathcal{E}_0$ may be positive. In this simulation, we notice that the maximum value of $\mathcal{E}_0$ is independent of the mesh refinement.

The third stationary solution concerns the transcritical flow without shock. This simulation is obtained by adopting the following initial data:

$$h(x,0) = 0.66 - z(x) \quad \text{and} \quad u(x,0) = 0. \tag{56}$$

The boundary conditions are given by:

$$h(0,t)u(0,t) = h(25,t)u(25,t) = 1.53 \quad \text{and} \quad h(25,t) = 0.66$$

while $h(0,t)$ is given by an usual Newman condition.

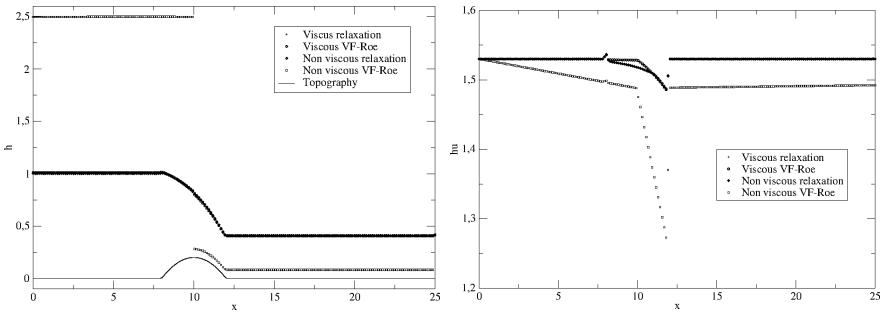

Figure 8: Numerical simulation obtained for the transcritical flow without shock at time $t = 200$ with 200 cells.

The obtained numerical results are displayed Figure 8. We notice that the numerical solution, obtained by the original (non viscous) VF-Roe scheme, contains a strong shock discontinuity violating the entropy stability.

Cells	Non viscous relaxation			Viscous relaxation			
	L^2-error	$max(\mathcal{E}_0)$	N	L^2-error	$\max_{n>0}\gamma^n$	$\bar{\gamma}$	N (increase)
200	2.4698E-3	1.5090E-3	20276	2.4698E-3	33732.41	0.4498	21655 (6%)
400	1.2152E-3	4.3561E-4	40816	1.2152E-3	58.95	0.1016	41429 (1%)
800	6.0196E-4	1.2171E-4	81893	6.0196E-4	123.75	6.3029E-2	82654 (0.9%)
1600	2.9948E-4	3.2614E-5	164047	2.9948E-4	3924.33	4.5342E-2	165154 (0.6%)

Table 4: Transcritical flow without shock at time $t = 200$ with the relaxation scheme. Evolution with respect to the cell number of the discharge L^2-error, the dissipation rate $\mathcal{E}_0$, the number of time iterations N and the percent increasing, the maximum value of γ^n and the average in time of γ^n.

Cells	L^2-error	$\max_{n>0}\gamma^n$	$\bar{\gamma}$	N
200	1.8791E-3	1473.34	0.2038	21018
400	8.8806E-4	793.23	0.1330	41778
800	4.3061E-4	334.02	8.5518E-2	83156
1600	2.1189E-4	13041.94	5.7416E-2	165818

Table 5: Transcritical flow without shock at time $t = 200$ with the viscous VF-Roe scheme. Evolution with respect to the cell number of the discharge L^2-error, the maximum value of γ^n and the average in time of γ^n.

We remark that the artificial viscosity technique clearly increases the stability of the scheme, in particular the VF-Roe scheme which now gives a correct approximate solution (see Table 5). Moreover, the expected entropy stability is reached with a neglecting amount of supplementary time iterations. Indeed, after Table 4 the entropy stability is get by adding a few percent of supplementary time iterations. Concerning the VF-Roe scheme, since it does not give a correct approximation with a vanishing viscosity, the comparison between viscous and non viscous approach is not relevant. However, we notice that the number of time iterations for the viscous VF-Roe scheme is very similar to the number of time iterations for the viscous Suliciu relaxation scheme. Once again, all these comments make the artificial viscosity technique very attractive.

The last stationary solution we simulate is the transcritical flow with shock. This numerical experiment is obtained by adopting the following initial data:

$$h(x,0) = 0.33 - z(x) \quad \text{and} \quad u(x,0) = 0. \tag{57}$$

The boundary conditions are given by

$$h(0,t)u(0,t) = h(25,t)u(25,t) = 0.18 \quad \text{and} \quad h(25,t) = 0.33$$

while $h(0,t)$ is given by an usual Newman condition.

The obtained numerical results are displayed Figure 9. Once again, we notice that the artificial viscosity increases the stability of the scheme, in particular the VF-Roe scheme which now gives a correct approximate solution (see Table 5). Moreover, the expected entropy stability is reached with a neglecting amount of supplementary time iterations as shown Table 6 and Table 7. Once again, this makes the artificial viscosity technique very attractive.

To conclude the steady state simulations, we adopt this last numerical experiment devoted to the transcritical flow with shock, to evaluate the behavior of the scheme with respect to the definition of the parameters $K_{i+\frac{1}{2}}$ and k, currently fixed by (48). In Table 8 and Table 9 we present the discharge L^2-error for several values of these parameters. We immediately notice that the approximate solution depends very weakly

Cells	Non viscous relaxation			Viscous relaxation			
	L^2-error	$max(\mathcal{E}_0)$	N	L^2-error	$\max_{n>0}\gamma^n$	$\bar{\gamma}$	N (increase)
200	8.7526E-4	9.2310E-3	10304	8.7526E-4	2307.32	5.3771E-3	10320 (0.1%)
400	4.9291E-4	9.2310E-3	21526	4.9291E-4	135.05	3.8418E-3	21550 (0.1%)
800	2.6938E-4	9.2310E-3	44271	2.6938E-4	37.66	1.9463E-3	44295 (0.05%)
1600	1.3965E-4	9.2310E-3	89571	1.3965E-4	37.61	1.9499E-3	89619 (0.05%)

Table 6: Transcritical flow with shock at time $t = 200$ with the relaxation scheme. Evolution with respect of the cell number of the discharge L^2-error, the dissipation rate $\mathcal{E}_0$, the number of time iterations N and the percent increasing, the maximum value of γ^n and the average in time of γ^n.

Cells	L^2-error	$\max_{n>0}\gamma^n$	$\bar{\gamma}$	N
200	8.4623E-4	80.86	6.7037E-2	10804
400	4.0205E-4	75.24	3.4464E-2	22114
800	2.1277E-4	106.62	1.7206E-2	44722
1600	1.080E-4	528.53	9.4965E-3	90001

Table 7: Transcritical flow with shock at time $t = 200$ with the viscous VF-Roe scheme. Evolution with respect to the cell number of the discharge L^2-error, the maximum value of γ^n and the average in time of γ^n.

$K_{i+\frac{1}{2}}$	Discharge L^2-error	
	Viscous relaxation	Viscous VF-Roe
$\min\left(1, \left(\frac{2}{u_i^n+u_{i+1}^n}\right)^2\right)$	2.2790E-3	2.2574E-3
$\min\left(10, \left(\frac{2}{u_i^n+u_{i+1}^n}\right)^2\right)$	3.1749E-3	3.1874E-3
$\min\left(\Delta x^2, \left(\frac{2}{u_i^n+u_{i+1}^n}\right)^2\right)$	4.9291E-4	4.0205E-4
$\min\left(\Delta x^4, \left(\frac{2}{u_i^n+u_{i+1}^n}\right)^2\right)$	4.9291E-4	4.0205E-4

Table 8: Transcritical flow with shock at time $t = 200$ with 400 cells. Discharge L^2-error versus the definition of $K_{i+\frac{1}{2}}$.

k	Discharge L^2-error	
	Viscous relaxation	Viscous VF-Roe
1	4.8110E-4	3.6097E-4
2	4.9291E-4	4.0205E-4
3	4.9367E-4	4.0431E-4
4	4.9371E-4	4.0445E-4

Table 9: Transcritical flow with shock at time $t = 200$ with 400 cells. Discharge L^2-error versus the definition of k involved in $\alpha_{i+\frac{1}{2}}$.

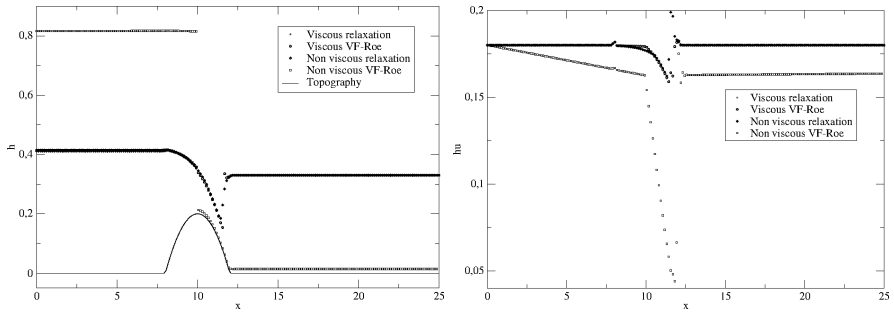

Figure 9: Numerical simulation obtained for the transcritical flow with shock discontinuity at time $t = 200$ with 200 cells.

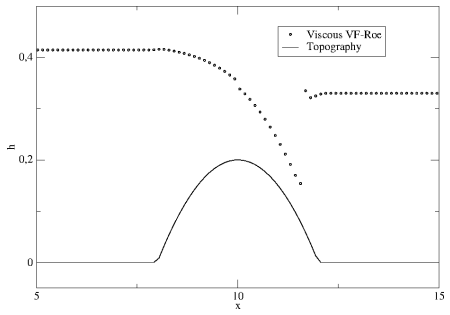

Figure 10: Numerical simulation of the hydraulic jump (zoom of the transcritical flow with shock discontinuity) at time $t = 200$ with 200 cells for the viscous VF-Roe scheme.

on the parameter k. Similarly, the dependence on the definition of $K_{i+\frac{1}{2}}$ is not crucial. However, we have a better approximation with a minimum value near zero. Moreover, here, we want to emphasize the very good approximation we obtain within the hydraulic jump as presented Figure 10. Indeed, it is worth noticing that the hydraulic jump is approximated with only one point for a nonpositive entropy dissipation rate $\mathcal{E}$.

5.3 Wet and dry transitions

In the two last simulations, we test the relevance of the viscosity technique when approximating wet and dry transitions. In the first simulation, we consider a dam-break over a flat topography. Then, we have fixed $z(x) = 0$. Here, the domain of computation is $[-10, 20]$. The numerical results are displayed Figure 11.

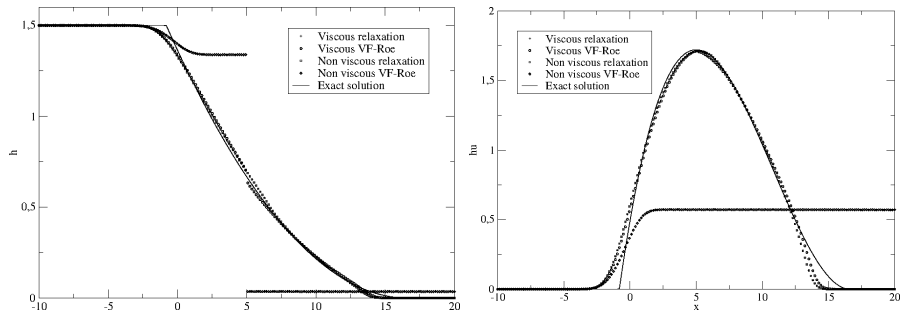

Figure 11: Numerical simulation obtained for dam-break over a dry area at time $t = 1.5$ with 200 cells.

Since the Suliciu relaxation scheme is entropy stable over a flat topography, the artificial viscosity stays inactive during the simulation and we get $\gamma^n = 0$. In Table 10, we exhibit the evolution of the L^2-error versus the number of cells. Concerning the

Cells	water height L^2-error	discharge L^2-error	N
200	1.3978E-2	4.0196E-2	132
400	8.5398E-3	2.5132E-2	278
800	5.0803E-3	1.5307E-2	581
1600	2.9665E-3	9.1340E-3	1204

Table 10: Dam-break over a dry area at time $t = 1.5$ with the relaxation scheme. Evolution with respect to the cell number of both water height and discharge L^2-error and the number of time iterations N.

Cells	L^2-error	$\max_{n>0} \gamma^n$	$\bar{\gamma}$	N
200	3.9049E-2	17.1792	0.1670	138
400	2.5349E-2	17.1792	0.1214	287
800	1.5729E-2	17.1792	8.1975E-2	592
1600	9.4474E-3	17.1792	5.2373E-2	1218

Table 11: Dam-break over a dry area at time $t = 1.5$ with the viscous VF-Roe scheme. Evolution with respect to the cell number of the discharge L^2-error, the maximum value of γ^n, the average in time of γ^n and the number of time iterations N.

non viscous VF-Roe scheme, once again, it is entropy violating and generates a wrong shock discontinuity. In Table 11, we give the evolution of the L^2-error, of the maximum value of γ^n and the average $\bar{\gamma^n}$. We notice that the needed number of time iterations if similar for both viscous schemes which indicates that the the artificial viscosity does not increase the time iterations. It is worth noticing that the suggested artificial viscosity approach is relevant to deal with dry areas over a flat topography to make it very attractive.

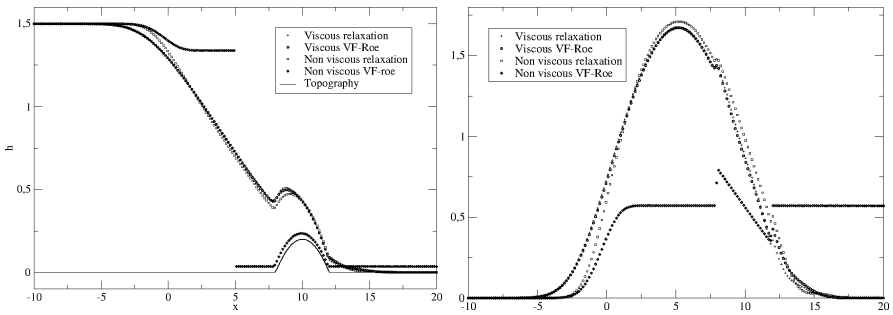

Figure 12: Numerical simulation obtained for dam-break over a bump at time $t = 1.5$ with 200 cells.

The last simulation we propose concerns a dam-break over a topography containing a bump as displayed Figure 12. Here the considered domain is $[-10, 20]$ while the topography function z is defined by (52). Because of the bump in the dry area, the viscosity parameter γ^n cannot be evaluated relevantly. Indeed, in the wet and dry transition, it is not possible to evaluate $\gamma^n \geq 0$ bounded such that the entropy dissipation rate $\mathcal{E}$, defined by (28), stays nonpositive. However, in order to perform this numerical experiment, we impose $\gamma^n = 0$ as soon as $\mathcal{D} = 0$. As a consequence, in this simulation, we are not able to enforce the required entropy inequality. However, as presented Table 12, the violation of the entropy dissipation rate remains very small and we may expect a correct convergence.

Cells	Viscous relaxation			Viscous VF-Roe		
	$max(\mathcal{E}_0 + \gamma^n \mathcal{D})$	$\bar{\gamma}$	N	$max(\mathcal{E}_0 + \gamma^n \mathcal{D})$	$\bar{\gamma}$	N
200	0.	9.3316	360	8.2667E-9	10.0568	323
400	3.8231E-8	4.9594	1228	7.2315E-9	12.5455	1021
800	1.7686E-5	6.0375	2094	1.4186E-6	24.9256	3279
1600	2.0661E-5	9.6409	5691	1.0098E-6	22.9878	7619

Table 12: Dam-break with dry area over a bump at time $t = 1.5$ with both viscous relaxation and VF-Roe schemes. Evolution of the entropy dissipation rate and the number of iteration versus the number of cells.

References

[1] E. Audusse, F. Bouchut, M.-O. Bristeau, R. Klein, and B. Perthame. A fast and stable well-balanced scheme with hydrostatic reconstruction for shallow water flows. *SIAM Journal on Scientific Computing*, 25(6):2050–2065, 2004.

[2] E. Audusse, F. Bouchut, M.-O. Bristeau, and J. Sainte-Marie. Kinetic entropy inequality and hydrostatic reconstruction scheme for the saint-venant system. *Mathematics of Computation*, 85(302):2815–2837, 2016.

[3] P. Azerad, J.-L. Guermond, and B. Popov. Well-balanced second-order approximation of the shallow water equation with continuous finite elements. *SIAM J. Numer. Anal.*, 55(6):3203–3224, 2017.

[4] A. Bermudez and M. E. Vazquez. Upwind methods for hyperbolic conservation laws with source terms. *Computers & Fluids*, 23(8):1049–1071, 1994.

[5] C. Berthon and C. Chalons. A fully well-balanced, positive and entropy-satisfying godunov-type method for the shallow-water equations. *Mathematics of Computation*, 85(299):1281–1307, 2016.

[6] C. Berthon and F. Marche. A positive preserving high order VFRoe scheme for shallow water equations: a class of relaxation schemes. *SIAM J. Sci. Comput.*, 30(5):2587–2612, 2008.

[7] F. Bouchut. *Nonlinear stability of finite volume methods for hyperbolic conservation laws and well-balanced schemes for sources.* Frontiers in Mathematics. Birkhäuser Verlag, Basel, 2004.

[8] F. Bouchut and T. Morales de Luna. A subsonic-well-balanced reconstruction scheme for shallow water flows. *SIAM Journal on Numerical Analysis*, 48(5):1733–1758, 2010.

[9] F. Bouchut and T. Morales de Luna. An entropy satisfying scheme for two-layer shallow water equations with uncoupled treatment. *M2AN Math. Model. Numer. Anal.*, 42(4):683–698, 2008.

[10] P. Cargo and A.-Y. Le Roux. Un schéma équilibre adapté au modèle d'atmosphère avec termes de gravité. *Comptes rendus de l'Académie des sciences. Série 1, Mathématique*, 318(1):73–76, 1994.

[11] G. Chen and S. Noelle. A new hydrostatic reconstruction scheme based on subcell reconstructions. *SIAM Journal on Numerical Analysis*, 55(2):758–784, 2017.

[12] F. Couderc, A. Duran, and J.-P. Vila. An explicit asymptotic preserving low Froude scheme for the multilayer shallow water model with density stratification. *Journal of Computational Physics*, 343:235–270, 2017.

[13] C.M. Dafermos. *Hyperbolic conservation laws in continuum physics*, volume 325 of *Grundlehren der Mathematischen Wissenschaften [Fundamental Principles of Mathematical Sciences]*. Springer-Verlag, Berlin, third edition, 2010.

[14] O. Delestre and P.-Y. Lagrée. A 'well-balanced' finite volume scheme for blood flow simulation. *Internat. J. Numer. Methods Fluids*, 72(2):177–205, 2013.

[15] E. D. Fernández-Nieto, J. Garres-Díaz, A. Mangeney, and G. Narbona-Reina. 2D granular flows with the $\mu(I)$ rheology and side walls friction: a well-balanced multilayer discretization. *J. Comput. Phys.*, 356:192–219, 2018.

[16] T. Gallouët, J.-M. Hérard, and N. Seguin. Some recent finite volume schemes to compute Euler equations using real gas EOS. *International journal for numerical methods in fluids*, 39(12):1073–1138, 2002.

[17] T. Gallouët, J.-M. Hérard, and N. Seguin. On the use of symmetrizing variables for vacuums. *Calcolo*, 40(3):163–194, 2003.

[18] E. Godlewski and P.-A. Raviart. *Hyperbolic systems of conservation laws*, volume 3/4 of *Mathématiques & Applications (Paris) [Mathematics and Applications]*. Ellipses, Paris, 1991.

[19] E. Godlewski and P.-A. Raviart. *Numerical approximation of hyperbolic systems of conservation laws*, volume 118 of *Applied Mathematical Sciences*. Springer-Verlag, New York, 1996.

[20] S.K. Godunov. A difference method for numerical calculation of discontinuous solutions of the equations of hydrodynamics. *Mat. Sb. (N.S.)*, 47(89):271–306, 1959.

[21] L. Gosse. A well-balanced flux-vector splitting scheme designed for hyperbolic systems of conservation laws with source terms. *Computers & Mathematics with Applications*, 39(9):135–159, 2000.

[22] N. Goutal and F. Maurel. *Proceedings of the 2nd workshop on dam-break wave simulation*. Electricité de France. Direction des études et recherches, 1997.

[23] N. Goutal and F. Maurel. Dam-break wave simulation. In *Proceedings of the First CADAM workshop*, 1998.

[24] J. M Greenberg and A.-Y. Leroux. A well-balanced scheme for the numerical processing of source terms in hyperbolic equations. *SIAM Journal on Numerical Analysis*, 33(1):1–16, 1996.

[25] J. M. Greenberg, A. Y. Leroux, R. Baraille, and A. Noussair. Analysis and approximation of conservation laws with source terms. *SIAM Journal on Numerical Analysis*, 34(5):1980–2007, 1997.

[26] N. Grenier, J.-P. Vila, and P. Villedieu. An accurate low-Mach scheme for a compressible two-fluid model applied to free-surface flows. *Journal of Computational Physics*, 252:1–19, 2013.

[27] A. Harten, P.D. Lax, and B. Van Leer. On upstream differencing and Godunov-type schemes for hyperbolic conservation laws. *SIAM review*, 25:35–61, 1983.

[28] S. Jin. A steady-state capturing method for hyperbolic systems with geometrical source terms. *ESAIM: Mathematical Modelling and Numerical Analysis*, 35(04):631–645, 2001.

[29] P.D. Lax. Shock waves and entropy. In *Contributions to nonlinear functional analysis (Proc. Sympos., Math. Res. Center, Univ. Wisconsin, Madison, Wis., 1971)*, pages 603–634. Academic Press, New York, 1971.

[30] P.D. Lax. *Hyperbolic systems of conservation laws and the mathematical theory of shock waves*, volume 11. SIAM, 1973.

[31] P.D. Lax and B. Wendroff. Systems of conservation laws. *Comm. Pure Appl. Math.*, 13:217–237, 1960.

[32] R.J. LeVeque. *Finite volume methods for hyperbolic problems*. Cambridge Texts in Applied Mathematics. Cambridge University Press, Cambridge, 2002.

[33] G. Li and Y. Xing. Well-balanced discontinuous Galerkin methods with hydrostatic reconstruction for the Euler equations with gravitation. *J. Comput. Phys.*, 352:445–462, 2018.

[34] Q. Liang and F. Marche. Numerical resolution of well-balanced shallow water equations with complex source terms. *Advances in water resources*, 32(6):873–884, 2009.

[35] J.-M. Masella, I. Faille, and T. Gallouët. On a rough godunov scheme. *Int. J. for Computational Fluid Dynamics*, 12(2):133–150, 1999.

[36] V. Michel-Dansac, C. Berthon, S. Clain, and F. Foucher. A well-balanced scheme for the shallow-water equations with topography. *Computers & Mathematics with Applications*, 72(3):568–593, 2016.

[37] V. Michel-Dansac, C. Berthon, S. Clain, and F. Foucher. A well-balanced scheme for the shallow-water equations with topography or manning friction. *Journal of Computational Physics*, 335:115–154, 2017.

[38] T. Morales, M. J. Castro Díaz, and C. Parés. Reliability of first order numerical schemes for solving shallow water system over abrupt topography. *Applied Mathematics and Computation*, 219(17):9012–9032, 2013.

[39] B. Perthame and C. Simeoni. A kinetic scheme for the Saint-Venant system with a source term. *Calcolo*, 38(4):201–231, 2001.

[40] P. L. Roe. Approximate Riemann solvers, parameter vectors, and difference schemes. *J. Comput. Phys.*, 43(2):357–372, 1981.

[41] D. Serre. *Systems of conservation laws. 1*. Cambridge University Press, Cambridge, 1999. Hyperbolicity, entropies, shock waves, Translated from the 1996 French original by I. N. Sneddon.

[42] E. Tadmor. Numerical viscosity and the entropy condition for conservative difference schemes. *Mathematics of Computation*, 43(168):369–381, 1984.

[43] E. Tadmor. The numerical viscosity of entropy stable schemes for systems of conservation laws. i. *Mathematics of Computation*, 49(179):91–103, 1987.

[44] E Tadmor. Entropy stable schemes. *Handbook of Numerical Methods for Hyperbolic Problems: Basic and Fundamental Issues, edited by R. Abgrall and C.-W. Shu (North-Holland, Elsevier, Amsterdam, 2017)*, 17:467–493, 2016.

[45] E.F. Toro. *Riemann solvers and numerical methods for fluid dynamics*. Springer-Verlag, Berlin, third edition, 2009. A practical introduction.

[46] E.F. Toro, M. Spruce, and W. Speares. Restoration of the contact surface in the HLL-Riemann solver. *Shock waves*, 4(1):25–34, 1994.